Mathematical Statistician and Engineering Applications
ISSN: 2094-0343
2326-9865

Power Transfer Matrix Model and SVPWM Technique Based Multi Variable Control Method for DFIG Wind Energy System

Dr B Mouli Chandra,
Professor and HoD, Department of EEE, QIS College of Engineering and Technology, Ongole email: bmoulichandra@gmail.com
Dr S. Muqthiar Ali,
Associate Professor, Dept. of EEE, A.I.T.S-Rajampet, A.P, INDIA
T Sreenivasa Murthy, Dr. R. Shankar,
Dept. of EEE, A.I.T.S-Rajampet, A.P, INDIA

Article Info
Page Number: 9944 – 9955
Publication Issue:
Vol 71 No. 4 (2022)

Abstract: — This paper gives an overview of Modeling and simulation of Doubly Fed Induction generator (DFIG) coupled with wind turbine using SVPWM technique. The power transfer matrix model uses instantaneous real/reactive power theory to improve the stability of power, which is injected by the wind energy to the power system. A power/current limiting scheme is also presented to protect power converters during a fault. Because of the advantages of the DFIG over other generators it is being used for most of the wind applications. Various researches have been done in modeling and simulation field of DFIG coupled with wind turbine. This paper summarizes the researches in the area of study of DFIG, steady state and transient analysis, its modeling, simulation, reactive power control strategies and performance analysis of DFIG coupled with wind turbine. The control schemes of DFIG are modelled and simulated in MATLAB/SIMULINK.

Article History
Article Received*: 15 September 2022*
Revised: *25 October 2022*
Accepted: *14 November 2022*
Publication: *21 December 2022*

I. INTRODUCTION

Worldwide concern about the environmental pollution and a possible energy crisis has led to increasing interest in technologies for generation of clean and renewable electrical energy. Among various renewable energy sources, wind power is the most rapidly growing one.

Much research effort has gone into modeling the DFIG wind turbines and studying their impact on the dynamic performance of the power system. In these works, the power electronic converter models are simplified as controlled ideal voltage-sources or current-sources. This permits large integration time-steps during transient simulations, which is essential in the representation of large networks. However, in the DFIG wind turbine system, the VFC and its power electronics (IGBT-switches) are the most sensitive part to grid disturbances. A question that arises is whether the simplified models of the VFC adequately represent its behavior during transient conditions. At the most detailed level, the operation of individual IGBT switches is fully represented. This level of modeling is useful for the detailed study of the power converter and its control strategy, and confirming the results of various simplified models. However, since the IGBT components in the VFC are switched on and off at a high frequency (several kHz or higher), it requires a very small simulation time-step (typically 10-50 μs) to accurately represent the PWM waveforms. This detailed switching-level (SL) model uses excessive computation time and is unsuitable for dynamic and transient study of large power systems with a high-level penetration of DFIG wind turbines.

This paper presents a modeling and control approach which uses instantaneous real and reactive power instead of dq components of currents in a vector control scheme. The main features of the proposed model compared to conventional models in the *dq* frame of reference are as follows.

1) *Robustness:* The waveforms of power components are independent of a reference frame; therefore, this approach is inherently robust against unaccounted dynamics such as PLL.

2) *Simplicity of realization:* The power components (state variables of a feedback control loop) can be directly obtained from *abc* phase voltage/current quantities, which simplify the implementation of the control system. Using power components instead of current in the model of the system, the control system requires an additional protection algorithm to prevent over current during a fault. Such an algorithm can be simply added to the control system via measuring the magnitude of current. The sequential loop closing technique is adopted to design a multivariable control system including six compensators for a DFIG wind energy system.

II. GENERAL FORM OF GENERATION SYSTEM

The general scheme of electrical energy's generation from the wind power on the basis of using doubly-fed induction generator is shown in Figure 1. The stator is considered to be connected to the grid directly whereas the rotor is connected to
it via back-to-back converter. Rotor side converter is a current regulate-voltage source inverter and grid side converter is a PWM inverter.

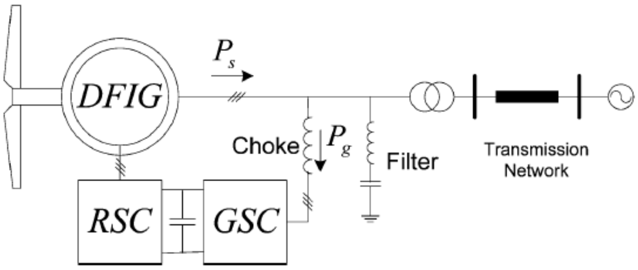

Fig. 1 General form of electrical energy's generation from the Wind Power on the induction generator

III. MODEL AND EQUATIONS OF WIND TURBINE USING POWER COMPONENTS

The schematic diagram of a DFIG wind turbine generator is depicted in Fig. 1. The power converter includes a rotor-side converter (RSC) to control the speed of generator and a grid-side converter (GSC) to inject reactive power to the system. Using a passive sign convention, the instantaneous real and reactive power components of the grid-side converter, $p_g(t)$ and $q_g(t)$ in the synchronous reference frame are

$$\begin{bmatrix} p_g(t) \\ q_g(t) \end{bmatrix} = \frac{3}{2} \begin{bmatrix} v_{sd} & v_{sq} \\ v_{sq} & -v_{sd} \end{bmatrix} \begin{bmatrix} i_{gd} \\ i_{gq} \end{bmatrix} \qquad (1)$$

Where $v_{sd,sq}$ and $i_{gd,gq}$ are *dq* components of the stator voltages
and GSC currents in the synchronous reference frame, respectively. Solving (1) for i_{gd} and i_{gq} , we obtain

$$\begin{bmatrix} i_{gd} \\ i_{gq} \end{bmatrix} = K_v \begin{bmatrix} p_g(t) \\ q_g(t) \end{bmatrix} \qquad (2)$$

Where

$$K_v = \frac{2}{3|v_s|^2} \begin{bmatrix} v_{sd} & v_{sq} \\ v_{sq} & -v_{sd} \end{bmatrix}, \quad |v_s| = \sqrt{v_{sq}^2 + v_{sd}^2}. \qquad (3)$$

Similarly, the instantaneous real/reactive power components of DFIG can be obtained in terms of stator currents as

$$\begin{bmatrix} p_s(t) \\ q_s(t) \end{bmatrix} = -\frac{3}{2} \begin{bmatrix} v_{sd} & v_{sq} \\ v_{sq} & -v_{sd} \end{bmatrix} \begin{bmatrix} i_{sd} \\ i_{sq} \end{bmatrix} \qquad (4)$$

and the stator current components are given by

$$\begin{bmatrix} i_{sd} \\ i_{sq} \end{bmatrix} = -K_v \begin{bmatrix} p_s(t) \\ q_s(t) \end{bmatrix}. \qquad (5)$$

The negative sign in (5) complies the direction of the stator power flow on Fig. 1. The exact dynamic model of an induction machine is conventionally expressed by voltage and torque equations. Herein, we develop a simplified model for the DIFG-based wind turbine of Fig. 1 by substituting currents in the exact model in terms of instantaneous real and reactive power.

A. Model of DFIG using Instantaneous power components

The voltage and flux equations of a doubly fed induction machine in the stator voltage synchronous reference frame can be summarized as

$$\mathbf{v}_{sdq} = r_s \mathbf{i}_{sdq} + j\omega_e \boldsymbol{\psi}_{sdq} + \frac{a\boldsymbol{\psi}_{sdq}}{dt} \quad (6)$$

$$\mathbf{v}_{rdq} = r_r \mathbf{i}_{rdq} + j\omega_{sl} \boldsymbol{\psi}_{rdq} + \frac{d\boldsymbol{\psi}_{rdq}}{dt} \quad (7)$$

$$\boldsymbol{\psi}_{sdq} = L_s \mathbf{i}_{sdq} + L_m \mathbf{i}_{rdq}, \quad \boldsymbol{\psi}_{rdq} = L_m \mathbf{i}_{sdq} + L_r \mathbf{i}_{rdq} \quad (8)$$

where r_s and r_r are the stator and rotor resistances, and w_s is the synchronous (stator) frequency. Subscripts s and r signify the stator and rotor variable, L_s , L_r *and* L_m are the stator, rotor, and magnetization inductances, respectively. The complex quantities V_{dq} ,i_{dq} and ψ_{dq} represent the voltage, current, and flux vectors, and w_{sl} is the slip frequency defined as

$$\mathbf{v}_{sdq,rdq} \triangleq v_{sd,rd} + jv_{sq,rq}, \quad \mathbf{i}_{sdq,rdq} \triangleq i_{sd,rd} + ji_{sq,rq};$$
$$\boldsymbol{\psi}_{sdq,rdq} \triangleq \psi_{sd,rd} + j\psi_{sq,rq}, \quad \omega_{sl} \triangleq \omega_e - \omega_r \quad (9)$$

where w_r is the rotor speed of the induction machine. To obtain a model of DFIG in terms of p(t) and q(t), the rotor flux and current are obtained from (8) as

$$\mathbf{i}_{rdq} = \frac{\boldsymbol{\psi}_{sdq} - L_s \mathbf{i}_{sdq}}{L_m}, \quad \boldsymbol{\psi}_{rdq} = \frac{L_r}{L_m}(\boldsymbol{\psi}_{sdq} - L'_s \mathbf{i}_{sdq}) \quad (10)$$

Where $L'_s \triangleq (1-(L_m^2)/(L_s L_r))L_s$. Then, by substituting for $\boldsymbol{i}_{rdq}$ and $\boldsymbol{V}_{rdq}$ from (10) in (7) and then by solving (6) and (7) for $\boldsymbol{i}_{sdq}$, we obtain

$$\frac{d}{dt}\mathbf{i}_{sdq} = \frac{1}{L'_s}\mathbf{v}_{sdq} - \frac{L_m}{L'_s L_r}\mathbf{v}_{rdq} + \frac{r_r - j\omega_r L_r}{L'_s L_r}\boldsymbol{\psi}_{sdq} - \left(\frac{r_r L_s + r_s L_r}{L_r L'_s} + j\omega_{sl}\right)\mathbf{i}_{sdq}. \quad (11)$$

Using (5) to replace $\boldsymbol{i}_{sd,sq}$ components of $\boldsymbol{i}_{sdq}$ in (11) and by rearranging the equation, we obtain

$$\frac{dp_s}{dt} = g_1 p_s - \omega_{sl} q_s - g_4 \psi_{sd} - g_5 \psi_{sq} + u_{rd} \quad (12)$$

$$\frac{dq_s}{dt} = \omega_{sl} p_s + g_1 q_s - g_5 \psi_{sd} + g_4 \psi_{sq} + u_{rq} \quad (13)$$

where

$$\begin{aligned} u_{rd} &= g_2 v_{rd} + g_3 v_{rq} - \frac{3|v_s|^2}{2L'_s} \\ u_{rq} &= g_3 v_{rd} - g_2 v_{rq}, \\ g_1 &= -\frac{r_s L_r + L_s r_s}{L'_s L_r}, \quad g_2 = \frac{3L_m v_{sd}}{2L_r L'_s} \\ g_3 &= \frac{3L_m v_{sq}}{2L_r L'_s} \\ g_4 &= \frac{3}{2}\left(\frac{r_r v_{sd} - L_r \omega_r v_{sq}}{L'_s L_r}\right) \\ g_5 &= \frac{3}{2}\left(\frac{r_r v_{sq} + L_r \omega_r v_{sd}}{L'_s L_r}\right). \end{aligned} \quad (14)$$

The state equation of the stator flux can be obtained by substituting for $\boldsymbol{i}_{sq}$ and $\boldsymbol{i}_{sd}$ from (5) in (6). Solving the stator voltage equations for $\psi_{sd,sq}$ yields

$$\frac{d\psi_{sd}}{dt} = v_{sd} + \omega_e \psi_{sq} + \frac{2r_s}{3|v_s|^2}(v_{sd}p_s + v_{sq}q_s) \quad (15)$$

$$\frac{d\psi_{sq}}{dt} = v_{sq} - \omega_e \psi_{sd} + \frac{2r_s}{3|v_s|^2}(v_{sq}p_s - v_{sd}q_s). \quad (16)$$

The electromechanical dynamic model of the machine is

$$\frac{d\omega_r}{dt} = \frac{P}{J}(T_e - T_m) \quad (17)$$

where P, J and T_m are the number of pole pairs, inertia of the rotor, and mechanical torque of the machine, respectively. The electric torque is given by

$$T_e = \frac{3}{2}P(\psi_{sd}i_{sq} - \psi_{sq}i_{sd}). \quad (18)$$

In (17), the mechanical torque T_m is input to the model and T_c based on (18), can be expressed in terms of instantaneous real and reactive power. Substituting for $\boldsymbol{i_{sd}}$ and $\boldsymbol{i_{sd}}$ from (5) in (18) and then replacing T_c in (17), we deduce

$$\frac{d\omega_r}{dt} = g_6 p_s + g_7 q_s - \frac{P}{J}T_m \quad (19)$$

where

$$g_6 = \frac{P^2}{J}\frac{\psi_{sq}v_{sd} - \psi_{sd}v_{sq}}{{v_s}^2}$$

$$g_7 = \frac{P^2}{J}\frac{\psi_{sd}v_{sd} + \psi_{sq}v_{sq}}{{v_s}^2} \quad (20)$$

The simplified model of the induction machine is presented in (12)–(16) and (19) which is summarized as

$$\frac{d}{dt}\begin{bmatrix} p_s \\ q_s \\ \psi_{sd} \\ \psi_{sq} \\ \omega_r \end{bmatrix} = \begin{bmatrix} g_1 & -\omega_{sl} & -g_4 & -g_5 & 0 \\ \omega_{sl} & g_1 & -g_5 & g_4 & 0 \\ \frac{2r_s v_{sd}}{3|v_s|^2} & \frac{2r_s v_{sq}}{3|v_s|^2} & 0 & \omega_e & 0 \\ \frac{2r_s v_{sq}}{3|v_s|^2} & -\frac{2r_s v_{sd}}{3|v_s|^2} & -\omega_e & 0 & 0 \\ g_6 & g_7 & 0 & 0 & 0 \end{bmatrix} \times \begin{bmatrix} p_s \\ q_s \\ \psi_{sd} \\ \psi_{sq} \\ \omega_r \end{bmatrix} + \begin{bmatrix} u_{rd} \\ u_{rq} \\ v_{sd} \\ v_{sq} \\ \frac{PT_m}{-J} \end{bmatrix} \quad (21)$$

The model of DFIG in (21) is a nonlinear dynamic model since the coefficients of the state variables are functions of the state variables.

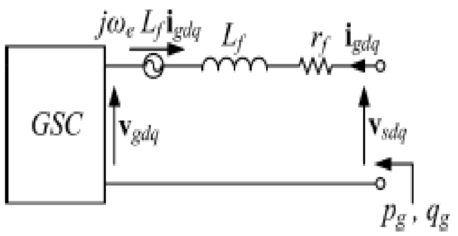

Fig. 2. Equivalent circuit of the grid-side filter.

B. Grid-side converter and filter model

Fig. 2 shows the representation of the grid-side converter and its filter in the synchronous reference frame. The *dq* model of the grid-side converter and filter is

$$\mathbf{v}_{sdq} = \mathbf{v}_{gdq} + L_f \frac{d\mathbf{i}_{gdq}}{dt} + j\omega_e L_f \mathbf{i}_{gdq} + r_f \mathbf{i}_{gdq} \quad (22)$$

where r_f and L_f are the resistance and inductance of the filter, respectively, and subscript signifies the variables at the gridside converter [19]. Substituting for i_{gdq} from (2) in (22) yields

$$\begin{bmatrix} \frac{dp_g}{dt} \\ \frac{dq_g}{dt} \end{bmatrix} = \begin{bmatrix} -\frac{r_f}{L_f} & -\omega_e \\ \omega_e & -\frac{r_f}{L_f} \end{bmatrix} \begin{bmatrix} p_g \\ q_g \end{bmatrix} + \begin{bmatrix} u_{gd} \\ u_{gq} \end{bmatrix} \quad (23)$$

where

$$u_{gd} = \frac{3}{2L_f}\left(|v_s|^2 - (v_{gd}v_{sd} + v_{gq}v_{sq})\right) \quad (24)$$

$$u_{gd} = \frac{3}{2L_f}(v_{gq}v_{sd} - v_{gd}v_{sq}). \quad (25)$$

The dc-link model can be deduced from the balance of real power at the converter dc-link node as given by

$$V_{dc}(t)I_{dc}(t) = p_g(t) - p_r(t) - p_{loss}(t) \quad (26)$$

Where p_r (t) is the real power that the converter delivers to the rotor and p_{loss} represents the total power loss, including converter switching losses and copper losses of the filter. The delivered real power to the rotor is

$$p_r = \frac{3}{2}(v_{rd}i_{rd} + v_{rq}i_{rq}) \quad (27)$$

Using (10) and (5), p_r can be expressed as

$$p_r = \frac{L_s(v_{sd}v_{rd} + v_{sq}v_{rq})}{L_m|v_s\ ^2} p_s + \frac{L_s(v_{sq}v_{rd} - v_{sd}v_{rq})}{L_m\ v_s|^2} q_s + \frac{3v_{rd}}{2L_m}\psi_{sd} + \frac{3v_{rq}}{2L_m}\psi_{sq}. \quad (28)$$

In the high-power converter, the power loss is often less than 1% of the total transferred power, and the impact of p_{loss} in (26) can be neglected. Substituting I_{dc} (t) = C (dV_{dc}(t))/dt in (26), the model of the dc link is deduced as follows:

$$\frac{dV_{dc}}{dt} = \frac{I_{dc}}{C} = \frac{p_g - p_r}{CV_{dc}}. \quad (29)$$

Using (28), the right-hand-side quantities in (29) can be expressed in terms of the state variables p_s, q_s, p_g, ψ_{sq}, ψ_{sd}

C. Wind Turbine Model

The captured mechanical power by a wind turbine can be expressed with the algebraic aerodynamic equation as

$$P_m = \frac{1}{2}C_P(\lambda,\beta)\rho\pi R^2 V_w^3 \quad (30)$$

where R, ρ, V_w are the wind turbine radius, air mass density, and wind speed, respectively. C_P is the wind turbine power coefficient which is a function of the tip speed ratio

$\lambda = R_\omega / V_w$ the pitch angle of the turbine blades, β . For a high-power wind turbine, the maximum mechanical power captured at λ_{opt} ranges from 6 to 8. Theoretically, it can be shown

$C_P < 0.6$ and practically at C_P is about 0.5 for high-power wind turbines.

IV. MULTIVARIABLE CONTROLLER DESIGN FOR A DFIG WIND TURBINE GENERATOR

Fig. 3 depicts the suggested multivariable feedback control system for the machine- and grid-side control schemes. In this scheme, the control inputs of the linearized model of the system are (u_{rd}, u_{rq}) to control real/reactive power of the rotor; and (u_{gd}, u_{gq}) to adjust the dc-link voltage and injected reactive power to the system. The feedback control system includes six compensators which are used in two nested loops. The inner loops consist of G_{Ps}, G_{Qs}, G_{Pg} and G_{Qg} where the required reactive power of the machine and grid are directly controlled via G_{Qs} and G_{Qg} control loops as shown Fig. 3. The outer control loops include $G_{\omega r}$ for regulating the rotor speed and G_{dc} for adjusting the dc-link voltage level.

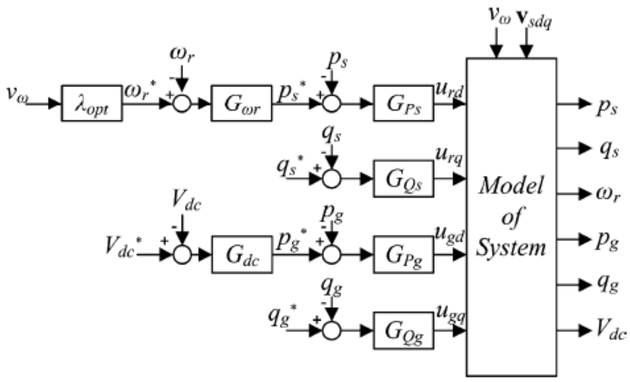

Fig. 3. Schematic diagram of the feedback control system for the machine-side and grid-side converters.

The sequential loop closing (SLC) method is adopted to design six controllers based on the multivariable model of the system developed in Section III. In the SLC method, based on physical relevance of the inputs and outputs, the input-output pairs are determined. Then, a controller is designed for the first pair of the input-output by treating the system as a single-input single-output (SISO) system.

Design of Controllers

1) Stator Real and Reactive Power Controllers: Considering $(\tilde{u}_{rd}, P_s)$ as the first pair in and, thus, imposing U_{rq}=0, we obtain the first SISO subsystem for controller design as

$$\tilde{p}_s = h_{11}\tilde{u}_{rd} \tag{31}$$

The first controller to be designed is

$$\tilde{u}_{rd} = G_{P_s}(\tilde{p}_s^* - \tilde{p}_s) \tag{32}$$

Substituting from (32) in (31), the closed-loop model of the first subsystem in Laplace domain is

$$\tilde{p}_s = \frac{h_{11}G_{P_s}}{1 + h_{11}G_{P_s}}\tilde{p}_s^* \tag{33}$$

Thus, G_{Ps} must be designed so that all poles of (33) remain in the left-half plane (LHP). The design of G_{Ps} can be simply performed via SISO system design methods, such as frequency response or root locus. To design G_{Qs} for reactive power control, the first controller G_{Ps} is considered as a part of the system, then by substituting for

$\tilde{u}_{rd} = G_{P_s}(\tilde{p}_s^* - \tilde{p}_s)$ and $\tilde{u}_{rq} = G_{Q_s}(\tilde{q}_s^* -$ q_s)in $\begin{bmatrix}\tilde{p}_s\\ \tilde{q}_s\\ \tilde{\omega}_r\end{bmatrix} = \begin{bmatrix}h_{11} & h_{12}\\ h_{21} & h_{22}\\ h_{31} & h_{32}\end{bmatrix}\begin{bmatrix}\tilde{u}_{rd}\\ \tilde{u}_{rq}\end{bmatrix}$ (34)

The closed-loop model of the second subsystem is obtained

$$\tilde{q}_s = \frac{G_1}{1 + G_2G_{Q_s}}\tilde{p}_s^* + \frac{G_1G_{Q_s}}{1 + G_2G_{Q_s}}\tilde{q}_s^* \tag{35}$$

where

$$G_1 = \frac{h_{21}G_{P_s}}{1 + h_{11}G_{P_s}}, \quad G_2 = h_{22} - \frac{h_{12}h_{21}G_{P_s}}{1 + h_{11}G_{P_s}}.$$

Thus, G_{Qs} must be designed so that the second subsystem in (35) remains stable.

2) Rotor Speed Controller: Speed control of the turbine-generator rotor is performed via control of the real power of the stator. Therefore, the speed controller $G\omega r$ uses p_s^* as the control input. Using the control scheme of Fig. 3, $p_s^*$is

$$\tilde{p}_s^* = G_{\omega_r}(\omega_r^* - \tilde{\omega}_r) \tag{36}$$

Embedding G_{Ps} and G_{Qs} controllers in the model of the system, the transfer function of rotor speed can be calculated as

$$\tilde{\omega}_r = G_3 p_s^* + G_4\tilde{q}_s^* \tag{37}$$

where

$$G_3 = \frac{h_{31}G_{P_s}(1+G_{Q_s}(G_1+G_2))}{(1+h_{11}G_{P_s})(1+G_2G_{Q_s})} - \frac{h_{32}G_{Q_s}G_1}{1+G_2G_{Q_s}},$$
$$G_4 = \frac{h_{32}G_{Q_s}}{1+G_2G_{Q_s}} - \frac{h_{12}h_{31}G_{P_s}^2}{(1+h_{11}G_{P_s})(1+G_2G_{Q_s})}.$$

Substituting p_s^* for from (36) in (37) yields

$$\tilde{\omega}_r = \frac{G_3G_{\omega_r}}{1+G_3G_{\omega_r}}\tilde{\omega}_r^* + \frac{G_4}{1+G_3G_{\omega_r}}\tilde{q}_s^*. \quad (38)$$

Thus, $G_{\omega r}$ must be designed so that the subsystem in (38) remains stable.

V. MODEL VALIDATION AND PERFORMANCE EVALUATION OF THE MULTIVARIABLE CONTROL SYSTEM

Fig. 4 shows the schematic of a study system for validation of the proposed modeling and control approaches. The study system includes a 1.5-MW DFIG wind turbine-generator connected to a grid. The electrical and mechanical parameters of the turbine generator are adopted from and summarized below.

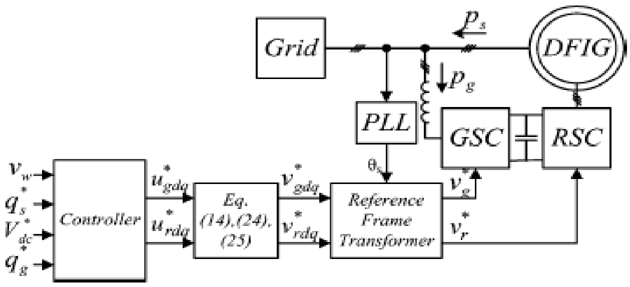

Fig. 4. Schematic diagram of the study system.

This system was tested under the following conditions:

1) Rated Power	1.5 [MW]
2) Rated Voltage (line to line)	0.575 [kv]
3) Rated Frequency	60 [Hz]
4) Rated Wind Speed	12.0 [m/s]
5) Stator Resistance	1.4 [mΩ]
6) Rotor Resistance	0.99 [mΩ]
7) Stator leakage inductance	89.98 [µH]
8) Rotor leakage inductance	82.08 [µH]
9) Magnetization inductance	1.526 [mH]
10) Stator/rotor turns ratio	1

Using the proposed designed method; the following per-unitized controllers were designed for the study system.

$$G_{P_s} = 1.33\left(1+\frac{10}{s}+\frac{s}{166.25}\right)\left(\frac{1}{1+0.016s}\right)$$
$$G_{Q_s} = 2.65\left(1+\frac{10}{s}+\frac{s}{331.25}\right)\left(\frac{1}{1+0.0032s}\right)$$

$$G_{P_g} = 2.65\left(1+\frac{10}{s}\right), \quad G_{Q_g} = 2.65\left(1+\frac{10}{s}\right)$$

$$G_{dc} = 4.32\left(1+\frac{2}{s}\right), \quad G_{\omega_r} = 7.54\left(1+\frac{2}{s}\right).$$

The performance of these controllers was investigated based on time-domain simulations of the study system using the Matlab/ Simulink software tool.

VI. MATLAB MODELLING AND SIMULATION RESULTS

The simulation diagram for DFIG based wind energy system is shown in below fig 5. The stator of the wound rotor induction machine is connected to the three-phase grid and the rotor side is fed via the back-to-back IGBT voltage-source inverters with a common DC bus. The grid side converter controls the power flow between the DC bus and the AC side and allows the system to be operated in sub synchronous and super synchronous speed.

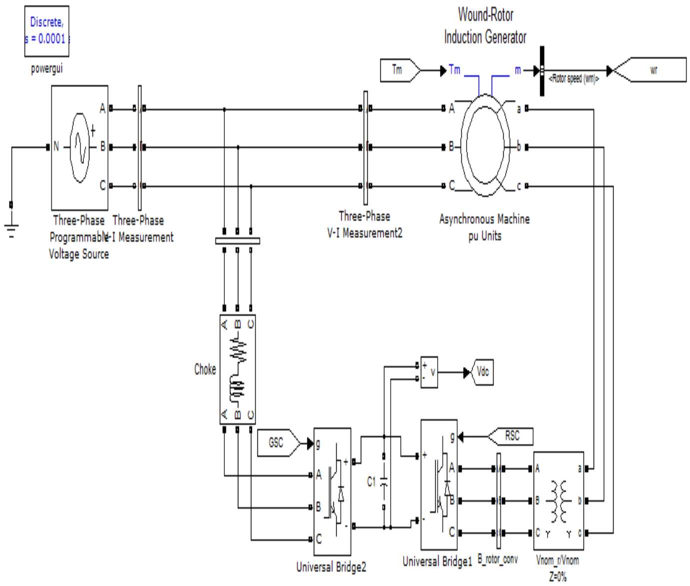

Fig. 5. Simulation diagram of DFIG based wind energy system

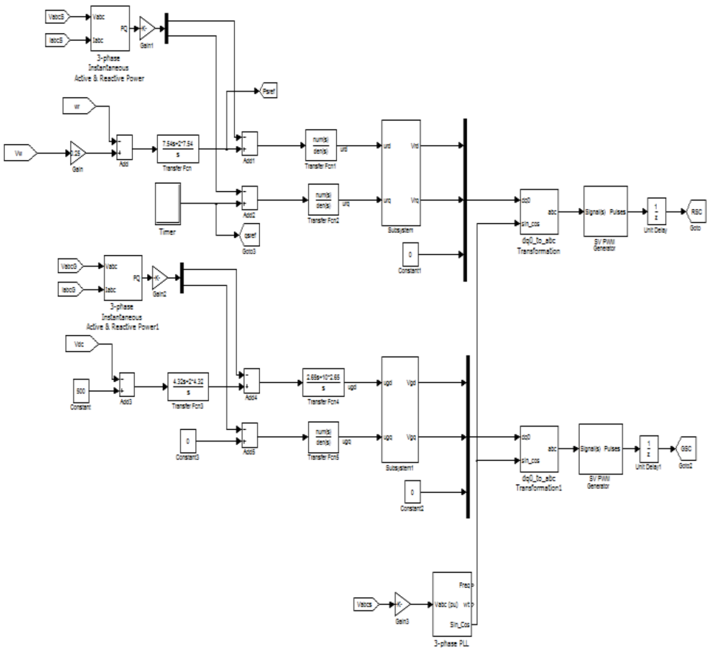

Fig. 6. Simulation diagram of DFIG controllers based on svpwm technique

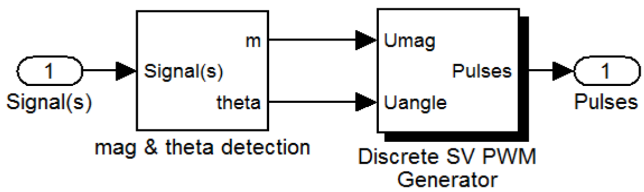

Fig. 7. Schematic representation of State Vector PWM

Fig 7. Shows the Space Vector PWM generation module accepts modulation index commands and generates the appropriate gate drive waveforms for each PWM cycle. The maximum achievable modulation (Umag_L) in the linear operating range is given by:

$$Umag\_L = 2^{25} * \sqrt{3} / Mod\_Scl$$

Over modulation occurs when modulation Umag>Umag_L. This corresponds to the condition where the voltage vector in increases. Under such circumstance, the Space Vector PWM algorithm will rescale the magnitude of the voltage vector to fit within the limit. However, the phase angle (θ) is always preserved. The transfer gain of the PWM modulator reduces and becomes non-linear in the over modulation region.

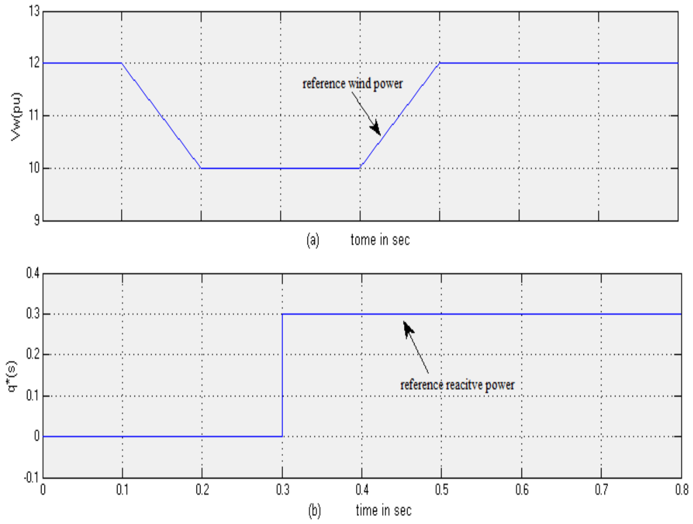

Fig. 8. Reference commands for wind and the stator reactive power.

Fig. 8(a) and 8(b) shows a trapezoidal pattern for wind speed and a step change in the reactive reference which are applied to the controllers of the study system. The trapezoidal pattern was selected to examine the system behavior following variation in the wind speed with both negative and positive slopes. Fig. 9 compares real/reactive power quantities of the DFIG against their command signals. Due to the coupling phenomenon, the variation of each power quantity can be considered as a disturbance to the other one.

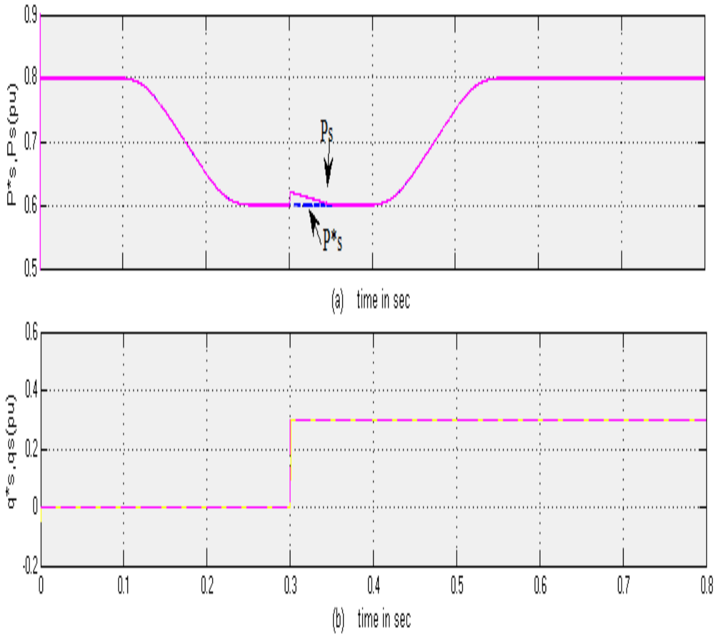

Fig. 9. Tracking performance of real and reactive stator powers

For instance, the effect of coupling can be seen in Fig. 9(a) at t=3 sec, where the step command in reactive power causes a small deviation in real power. However, as Fig. 9 shows, both real and reactive power quantities accurately track their command signals which mean the controllers successfully mitigate the impact of coupling effect in the tracking of commands signals.

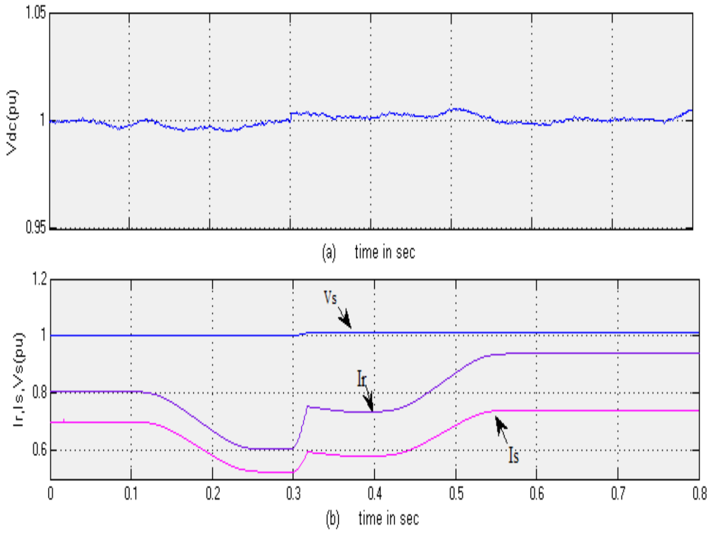

Fig. 10. RMS values of the stator voltage and currents.

Fig. 10(a) and (b) depicts the dc-link voltage and the rms values of the machine voltage/current quantities. These figures show that the stator and rotor currents are changing as the real/reactive power changes whereas the dc link and stator voltages remained fixed as expected from the control strategy. Specifically, the I_S and I_r current curves.

VII. CONCLUSION

From the simulation behavior of the actual DFIG. It is shown that the DFIG model approaches in order to fully evaluate the fault degrees when designing protection schemes and also for future research on improved control strategies and the fault ride through capability for DFIG-based wind power generation systems. The waveforms of the power components remain intact at different reference frames and can be easily calculated using the phase voltages and currents. Therefore, this approach facilitates the implementation of the controllers and improves the robustness of the control system.

The proposed approach is verified using the time-domain simulation of a study system for DFIG wind energy systems. The simulation results show that the suggested model and control scheme can successfully track the rotor speed reference for capturing the maximum power and maintain the dc-link voltage of the converter regardless of disturbances due to changes in real and reactive power references.

REFERENCES

[1] K. Xie and R. Billinton, “Determination of the optimum capacity and type of wind turbine generators in a power system,” *IEEE Trans. Energy Convers.*, vol. 26, no. 1, pp. 227–234, Mar. 2011.

[2] T. Zhou and B. François, “Energy management and power control of a hybrid active wind generator for distributed power generation and grid integration,” *IEEE Trans. Ind. Electron.*, vol. 58, no. 1, pp. 95–104, Jan. 2011.

[3] J. Hu, H. Nian, H. Xu, and Y. He, “Dynamic modeling and improved control of DFIG under distorted grid voltage conditions,” *IEEE Trans. Energy Convers.*, vol. 26, no. 1, pp. 163–175, Mar. 2011.

[4] Tabassum, Saleha, and B. Mouli Chandra. "Power Quality improvement by UPQC using ANN Controller." International Journal of Engineering Research and Applications 2.4 (2012): 2019-2024.

[5] Chandra, B. Mouli, and Dr S. Tara Kalyani. "FPGA controlled stator resistance estimation in IVC of IM using FLC." Global Journal of Researches in Engineering Electrical and Electronics Engineering 13.13 (2013).

[6] Chandra, B. Mouli, and S. Tara Kalyani. "Online identification and adaptation of rotor resistance in feedforward vector controlled induction motor drive." Power Electronics (IICPE), 2012 IEEE 5th India International Conference on. IEEE, 2012.
[7] Chandra, B. Mouli, and S. Tara Kalyani. "Online estimation of Stator resistance in vector control of Induction motor drive." Power India Conference, 2012 IEEE Fifth. IEEE, 2012.
[8] MURALI, S., and B. MOULI CHANDRA. "THREE PHASE 11-LEVEL INVERTER WITH REDUCED NUMBER OF SWITCHES FOR GRID CONNECTED PV SYSTEMS USING VARIOUS PWM TECHNIQUES."
[9] BABU, GANDI SUNIL, and B. MOULI CHANDRA. "POWER QUALITY IMPROVEMENT WITH NINE LEVEL MULTILEVEL INVERTER FOR SINGLE PHASE GRID CONNECTED SYSTEM."
[10] NAVEENKUMAR, K., and B. MOULI CHANDRA. "Performance Evaluation of HVDC Transmission system with the Combination of VSC and H-Bridge cells." Performance Evaluation 3.02 (2016).
[11] Vijayalakshmi, R., G. Naga Mahesh, and B. Mouli Chandra. "Seven Level Shunt Active Power Filter for Induction Motor Drive System." International Journal of Research 2.12 (2015): 578-583.
[12] BAI, RM DEEPTHI, and B. MOULI CHANDRA. "Speed Sensorless Control Scheme of Induction Motor against Rotor Resistance Variation." (2013).
[13] Chandra, B. Mouli, and S. Tara Kalyani. "Online Rotor Time Constant Tuning in Indirect Vector Control of Induction Motor Drive." International Journal on Engineering Applications (IREA) 1.1 (2013): 10-15.
[14] Rajesh, P., Shajin, F. H., Mouli Chandra, B., & Kommula, B. N. (2021). Diminishing Energy Consumption Cost and Optimal Energy Management of Photovoltaic Aided Electric Vehicle (PV-EV) By GFO-VITG Approach. Energy Sources, Part A: Recovery, Utilization, and Environmental Effects, 1-19.
[15] Reddy C, Narukullapati BK, Uma Maheswara Rao M, Ravindra S, Venkatesh PM, Kumar A, Ch T, Chandra BM, Berhanu AA. Nonisolated DC to DC Converters for High-Voltage Gain Applications Using the MPPT Approach. Mathematical Problems in Engineering. 2022 Aug 22;2022.
[16] Sravani, B., C. Moulika, and M. Prudhvi. "Touchless door bell for post-covid." South Asian Journal of Engineering and Technology 12.2 (2022): 54-56.
[17] Mounika, P., V. Rani, and P. Sushma. "Embedded solar tracking system using arduino." South Asian Journal of Engineering and Technology 12.2 (2022): 1-4.
[18] Prakash, A., Srikanth, T., Moulichandra, B., & Krishnakumar, R. (2022, February). Search and Rescue Optimization to solve Economic Emission Dispatch. In 2022 First International Conference on Electrical, Electronics, Information and Communication Technologies (ICEEICT) (pp. 1-5). IEEE.
[19] Kannan, A. S., Srikanth Thummala, and B. Mouli Chandra. "Cost Optimization Of Micro-Grid Of Renewable Energy Resources Connected With And Without Utility Grid." Materials Today: Proceedings (2021).
[20] Chandra, B. M., Sonia, D., Roopa Devi, A., Yamini Saraswathi, C., Mighty Rathan, K., & Bharghavi, K. (2021). Recognition of vehicle number plate using Matlab. J. Univ. Shanghai Sci. Technol, 23(2), 363-370.
[21] Noushin, S. K., and Daka Prasad2 Dr B. Mouli Chandra. "A Hybrid AC/DC Micro grid for Improving the Grid current and Capacitor Voltage Balancing by Three-Phase AC Current and DC Rail Voltage Balancing Method."
[22] Deepika, M., Kavitha, M., Chakravarthy, N. K., Rao, J. S., Reddy, D. M., & Chandra, B. M. (2021, January). A Critical Study on Campus Energy Monitoring System and Role of IoT. In 2021 International Conference on Sustainable Energy and Future Electric Transportation (SEFET) (pp. 1-6). IEEE.
[23] ANITHA, CH, and B. MOULI CHANDRA. "A SINGLE-PHASE GRID-CONNECTED PHOTOVOLTAIC INVERTER BASED ON A THREE-SWITCH THREE-PORT FLYBACK WITH SERIES POWER DECOUPLING CIRCUIT."
[24] Sai, V. N. V., Kumar, V. B. C., Kumar, P. A., Pranav, I. S., Venkatesh, R., Srinivasulu, T. S., ... & Chandra, B. M. Performance Analysis of a DC Grid-Based Wind Power Generation System in a Microgrid.
[25] Prakash, A., R. Anand, and B. Mouli Chandra. "Forward Search Approach using Power Search Algorithm (FSA-PSA) to solve Dynamic Economic Load Dispatch problems." 2019 5th International Conference on Advanced Computing & Communication Systems (ICACCS). IEEE, 2019.
[26] K Balasamy, N Krishnaraj, K Vijayalakshmi “Improving the security of medical image through neuro-fuzzy based ROI selection for reliable transmission” Journal of Multimedia Tools and Applications, Springer US, Page no. 14321-14337Vol:81, 4/2022.

[27] M. Jeyaselvi, C. Jayakumar, M. Sathya, S. J. A. Ibrahim and N. S. Kalyan Chakravarthy, "Cyber security-based Multikey Management System in Cloud Environment," 2022 International Conference on Engineering and Emerging Technologies (ICEET), Kuala Lumpur, Malaysia, 2022, pp. 1-6, doi:10.1109/ICEET56468.2022.10007104, https://ieeexplore.ieee.org/abstract/document/10007104

[28] S. Jafar Ali Ibrahim et al., "Rough set based on least dissimilarity normalized index for handling uncertainty during E-learners learning pattern recognition", International Journal of Intelligent Networks, Volume 3, 2022, Pages 133-137, ISSN 2666-6030, https://doi.org/10.1016/j.ijin.2022.09.001.(https://www.sciencedirect.com/science/article/pii/S2666603022000148)

[29] Ibrahim,S. Jafar Ali, Rajasekar S. Chakravarthy N. S. Kalyan, Varsha, Singh Maninder Pal , Kumar Vaneet and Saruchi Synthesis, Characterization of Ag/Tio2 Nanocomposite: Its Anticancer and Anti-Bacterial and Activities, Global Nest, Volume 24, Issue 2, June 2022, Pages:262-266, Issn No: 1790-7632, DOI: https://doi.org/10.30955/gnj.0042505

[30] Linjiang Xie, Feilu Hang, Wei Guo, Yao Lv, Wei Ou, and C. Chandru Vignesh "Machine learning-based security active defence model - security active defence technology in the communication network "International Journal of Internet Protocol Technology 2022 15:3-4, 169-181 https://doi.org/10.1504/IJIPT.2022.125955

[31] KexuWu, Chaolin Li, Chandru Vignesh C, Alfred Daniel J "Digital teaching in the context of Chinese universities and their impact on students for Ubiquitous Applications" Computers and Electrical Engineering, Volume 100, May 2022, 107951, https://doi.org/10.1016/j.compeleceng.2022.107951

[32] Huiyi Zang, C Chandru Vignesh and J Alfred Daniel "Influence of Social and Environmental Responsibility in Energy Efficiency Management for Smart City"Journal of Interconnection Networks, Vol. 22, No. Supp01, 2141002 (2022), https://doi.org/10.1142/S0219265921410024.

[33] R Menaha, VE Jayanthi, N Krishnaraj," A Cluster-based Approach for Finding Domain wise Experts in Community Question Answering System", Journal of Physics: Conference Series, Volume: 1767, IOP Publishing, 2021. DOI 10.1088/1742-6596/1767/1/012035.

[34] J Ramprasath, M Aswin Yegappan, Dinesh Ravi, N Balakrishnan and S Kaarthi, Assigning Static Ip Using DHCP In Accordance With MAC, INTERNATIONAL JOURNAL FOR TRENDS IN ENGINEERING & TECHNOLOGY, Vol 20, Issue 1, 2017.

[35] J Ramprasath, Dr S Ramakrishnan, P Saravana Perumal, M Sivaprakasam, U Manokaran Vishnuraj, Secure network implementation using VLAN and ACL, International Journal of Advanced Engineering Research and Science, Vol 3, Issue 1, PP. 2349-6495, 2016

[36] J Ramprasath, V Seethalakshmi, Secure access of resources in software-defined networks using dynamic access control list, International Journal of Communication Systems, Vol 34, Issue 1, PP. e4607, 2020

[37] Balasamy, K., Krishnaraj, N. & Vijayalakshmi, K. An Adaptive Neuro-Fuzzy Based Region Selection and Authenticating Medical Image Through Watermarking for Secure Communication. Wireless Pers Commun 122, 2817–2837 (2022). https://doi.org/10.1007/s11277-021-09031-9